Available online at www.sciencedirect.com
ScienceDirect
Journal of Nuclear Materials 374 (2008) 197–203
journal of nuclear materials
www.elsevier.com/locate/jnucmat

A superior corrosion behavior of Zircaloy-4 in lithiated water at 360 °C/18.6 MPa by β-quenching

M.Y. Yao [a,*], B.X. Zhou [a], Q. Li [b], W.Q. Liu [b], X. Geng [a], Y.P. Lu [a]

[a] Institute of Materials, Shanghai University, Box 269, No. 149 Yanchang Road, Shanghai 200072, PR China
[b] Key Laboratory for Advanced Micro-Analysis, Shanghai University, Shanghai 200444, PR China

Received 30 January 2007; accepted 6 August 2007

Abstract

To further understand the mechanism on the heat-treatment effect on corrosion behavior of Zircaloy-4, β-quenched and recrystallized specimens are corroded in an autoclave with 0.01 M LiOH aqueous solution at 360 °C/18.6 MPa. Results show that the β-quenched specimen possesses excellent corrosion resistance, the weight gain of which is consistently comparable to that of ZIRLO and N18 alloys during 529 days exposure, while the recrystallized specimen exhibits accelerated corrosion rate after 100 days exposure. The increase of the supersaturated solid solution contents of Fe and Cr in α-Zr matrix is responsible for the improvement of corrosion resistance by β-quenching treatment. The fracture surface and inner surface morphology of oxide films indicates that β-quenching treatment significantly slow down the development of pores to cracks in oxide films and reduces the uneven growing tendency of the oxide, which is related to the corrosion behavior.

1. Introduction

It is well known that the presence of LiOH in water at high temperature and pressure is detrimental to the corrosion resistance of Zircaloy-4 (denoted as Zry-4), increasing corrosion rate at the post-transition stage dramatically [1–6]. Although the corrosion resistance of Zry-4 in lithiated water can be further improved by optimizing the thermo-mechanical processing, it is still low compared to that of Zr–Sn–Nb alloys, such as ZIRLO (Zr–1Sn–1Nb–0.1Fe) [7,8], N18(Zr–1Sn–0.4Nb–0.3Fe–0.1Cr) [9] and E635 (Zr–1.2Sn–1Nb–0.4Fe) [10]. Considering that Nb has a higher solubility limit in α-Zr matrix (about 0.6% in mass fraction at 610 °C) [11]), the superior corrosion resistance of these Zr–Sn–Nb alloys in lithiated water reminds us whether increase of Fe and Cr contents in α-Zr matrix by supersaturated solid solution treatment, e.g., solution-treated by β-quenching, could further improve the corrosion resistance of Zry-4 in lithiated water.

So far, there is no general agreement on the reason for the impact of thermo-mechanical processing on the uniform corrosion behavior of Zry-4. Some researchers [12–14] attribute it to the size and distribution of $Zr(Fe,Cr)_2$ second phase particles (SPPs) since Fe and Cr alloying elements have low solubilities in α-Zr matrix (lower than 200 μg/g even at 810 °C with the maximum solubility) and precipitate as $Zr(Fe,Cr)_2$ SPPs [15]. However, others [16–19] ascribe it to the variation of Fe and Cr contents in α-Zr solid solution because they will also vary with the precipitation of $Zr(Fe,Cr)_2$ SPPs.

Hence, it is necessary to further study the corrosion behavior of Zry-4 specimens with different heat-treatments, especially solution-treated by β-quenching, in LiOH aqueous solution at 360 °C/18.6 MPa. Although it is impractical to employ such treatment at the final stage in manufacturing Zry-4 tubes, it is helpful for us to understand the corrosion mechanism affected by alloying elements and heat-treatments.

* Corresponding author. Tel.: +86 21 5633 7032; fax: +86 21 5633 3870.
E-mail address: yaomeiyi@shu.edu.cn (M.Y. Yao).

0022-3115/$ - see front matter © 2007 Elsevier B.V. All rights reserved.
doi:10.1016/j.jnucmat.2007.08.002

2. Experimental procedure

2.1. Specimens preparation and microstructure characterization

Specimens with 25 mm × 10 mm and 25 mm × 20 mm were cut from a Zry-4 (Zr–1.5Sn–0.2Fe–0.1Cr, mass fraction %) plate with 0.6 mm thickness, which was fabricated by conventional procedure [20] and underwent a final recrystallization anneal at 600 °C for 1 h (accumulated annealing parameter $\sum A_i = 4 \times 10^{-17}$ h, calculating from $\sum A_i = \sum t_i \exp(-40000/T_i)$). The specimens with 25 mm × 20 mm were not heat-treated any further (denoted as RA Zry-4). The specimens with 25 mm × 10 mm were sealed in an evacuated quartz capsule at about 5×10^{-3} Pa and solution-treated at 1020 °C (β phase) for 10 min, then quenched in water and broken the capsule simultaneously (denoted as βQ Zry-4).

The microstructure of the specimens with different heat-treatments was examined by JEM-200CX transmission electron microscope (TEM). Disk specimens, 3 mm in diameter, were mechanically grinded to about 70 μm in thickness, and then thinned by twin-jet electro-polishing technique at a voltage of 40–50 V in a mixture of 10% perchloric acid and 90% ethanol (in volume) at −40 °C. The contents of alloying elements in α-Zr matrix were measured using EDS fitted in a JEM-2010F TEM with live time of 1000 s.

2.2. Autoclave testing

The corrosion tests for these specimens were performed in an autoclave with 0.01 M LiOH aqueous solution at 360 °C/18.6 MPa. The weight gain was a mean value obtained from three specimens. Prior to the corrosion tests, the specimens were cleaned and pickled in a solution of 10% HF + 45% HNO_3 + 45% H_2O (in volume), sequentially rinsed in cold tap water, boiling deionized water and then blow-dried with warm air.

2.3. Fracture surface and inner surface characterization techniques

JSM-6700F high resolution scanning electron microscope (HRSEM) was used to characterize the morphology of fracture surface and inner surface of oxide films formed on specimens after corrosion. The preparation of fracture surface and inner surface samples have been described in Ref. [21] in detail. A schematic diagram of the specimen preparation is shown in Fig. 1. Firstly, the cross-section of the corroded specimen was etched in the same solution as pickling specimens for corrosion tests to dissolve the metal matrix and reveal the metal/oxide interface, and then the upstretched oxide film on the cross-section was broken off. The leaving cross-section sample was used for HRSEM examination of the fracture surface, while the broken oxide flake was used for HRSEM examination of the inner surface. In order to avoid charging by bombardment of electron beams in the microscope, a thin layer of gold was deposited on the oxide samples by sputtering.

3. Experimental results

3.1. The microstructure of Zry-4 specimens

Fig. 2 shows the microstructure of βQ Zry-4 and RA Zry-4 specimens. The SPPs in βQ Zry-4 specimen can be hardly distinguished during TEM examination at low magnification (10000×) (Fig. 2(a)), but at higher magnification (50000×), the fine SPPs (<0.05 μm) precipitated along the grain boundaries of lath-like α-Zr grains can be observed (indicated by an arrow in Fig. 2(b)). The SPPs in RA Zry-4 specimen are much larger in size (0.05–0.2 μm) and higher in quantity (Fig. 2(c)). The difference in size and quantity of SPPs indicates that higher Fe and Cr alloying elements should be supersaturated solid solution in α-Zr after β-quenching.

The results from EDS analysis are summarized in Table 1. From Table 1, the obvious difference in Fe and Cr contents in α-Zr matrix of the two groups of Zry-4 specimens can be seen. For βQ Zry-4 specimen, the contents of Fe and Cr in α-Zr matrix amount to about 700 μg/g, respectively, which are much higher than their maximal solubility in α-Zr matrix (120 μg/g for Fe and 200 μg/g for Cr [15]). For RA Zry-4 specimen, however, the contents of Fe and Cr in α-Zr matrix are too low to be detected. This illustrates that higher contents of Fe and Cr are indeed supersaturated solid solution in α-Zr after β-quenching, which is consistent with the result of SPPs observation. Moreover, the Sn content has no difference in the matrix of two

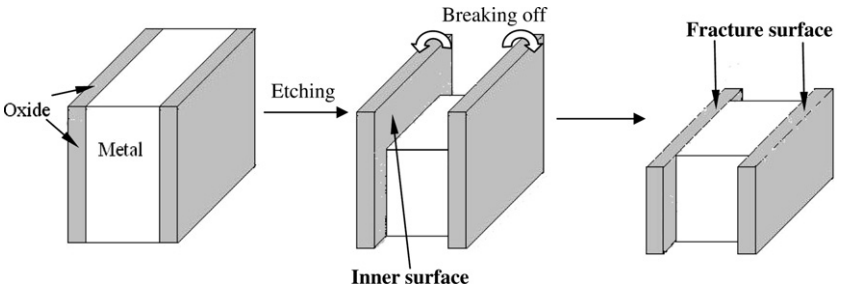

Fig. 1. A schematic diagram of the oxide specimen preparation for the examination of inner and fracture surface.

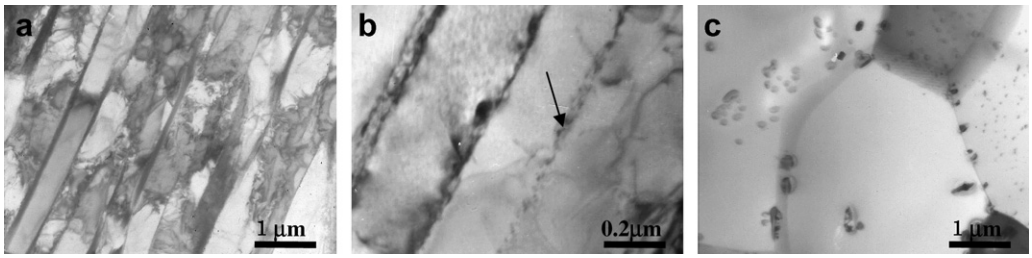

Fig. 2. The TEM micrographs of different specimens: (a, b) βQ Zry-4 with different magnifications and (c) RA Zry-4.

Table 1
The contents of alloying elements in α-Zr matrix in βQ Zry-4 and RA Zry-4 specimens

Specimens	Mean content		
	Fe (μg/g)	Cr (μg/g)	Sn (mass fraction %)
βQ Zry-4	700 ± 400	700 ± 300	1.44 ± 0.09
RA Zry-4	–	–	1.5 ± 0.03

groups of specimens and is close to that of Zry-4 alloy (1.5%). It shows that 1.5% Sn is completely in the solid solution of α-Zr matrix.

3.2. Corrosion behavior

Fig. 3 shows the corrosion weight gain as a function of exposure time after the autoclave tests in 0.01 M LiOH aqueous solution at 360 °C/18.6 MPa for the two groups of specimens. For comparison, the weight gain vs time of ZIRLO [8] and N18 tested in the same condition as this study and RA Zry-4 tested in deionized water at 360 °C/18.6 MPa is also presented in Fig. 3. Here, the weight gain data of ZIRLO in lithiated water and RA Zry-4 in pure water was taken from Refs. [8,21], respectively, while the data of N18 was obtained by corroding together with βQ Zry-4 and RA Zry-4 specimens in the same autoclave, which is close to Zhao's result [9]. Obviously, a very rapid

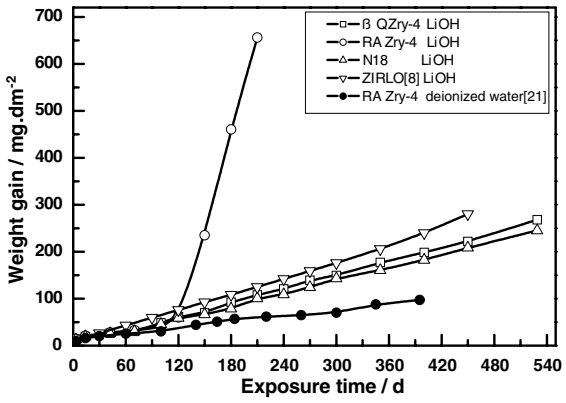

Fig. 3. Corrosion weight gain vs. exposure time of βQ Zry-4 and RA Zry-4 specimens tested in 0.01 M LiOH aqueous solution at 360 °C/18.6 MPa. The weight gain vs. time of ZIRLO [8] and N18 tested in the same condition as this study and RA Zry-4 tested in deionized water at 360 °C/18.6 MPa [21] is also presented here.

increase in the post-transition corrosion rate is observed in RA Zry-4 specimen in lithiated water environment. This is a general phenomenon for Zircaloy corroded in lithiated water. Based on the Li^+ incorporated in the oxide layer, some mechanisms were suggested by many researchers, e.g. preferential dissolution of cubic/tetragonal ZrO_2 to form a porous inner layer of oxide [22], the gradual alteration of the barrier layer properties [2,23], the modification of normal oxide growth by surface LiO groups [24,25], and reduction of the surface free energy of ZrO_2 to promote the formation of pores and cracks [26]. It is not further discussed here.

It is interesting and surprising that βQ Zry-4 specimen exhibits superior corrosion resistance in lithiated water. Compared to the post-transition corrosion rate of RA Zry-4 specimen in pure water, the corrosion rate in lithiated water is increased by only about a factor of 3 for βQ Zry-4 specimen, but about a factor of 33 for RA Zry-4 specimen. The weight gain of RA Zry-4 specimen has reached about 700 mg/dm^2 after 210 days exposure, while that of βQ Zry-4 specimen is only about 268 mg/dm^2 even after 529 days exposure. The weight gain of βQ Zry-4 specimen is consistently comparable to that of ZIRLO and N18 (Fig. 3), which exhibit superior corrosion resistance in lithiated water. This shows that the corrosion resistance of Zry-4 in lithiated water can be really further improved by solution-treatment.

3.3. Morphology of the fracture surface and inner surface of oxide films

3.3.1. Fracture surface morphology of oxide films

Fig. 4 shows the fracture surface morphology of the oxide films formed on RA Zry-4 and βQ Zry-4 specimens corroded in lithiated water for different time, respectively. At the early stage of oxide growth (100 days exposure), the oxide films on both RA Zry-4 and βQ Zry-4 specimens are compact and no large cracks are observed except for a few micro-cracks or pores (Fig. 4(a) and (d)). At the later stage of oxide growth (210 days exposure), the amount of cracks in the oxide film on RA Zry-4 specimen (indicated by arrows in Fig. 4(b)) is much more than that on βQ Zry-4 specimen (Fig. 4(e)). At high magnification, more pores can be observed in RA Zry-4 specimen than in βQ Zry-4 specimen (Fig. 4(c) and (f)). Here, the cracks are likely an artifact of sample preparation, but the locations

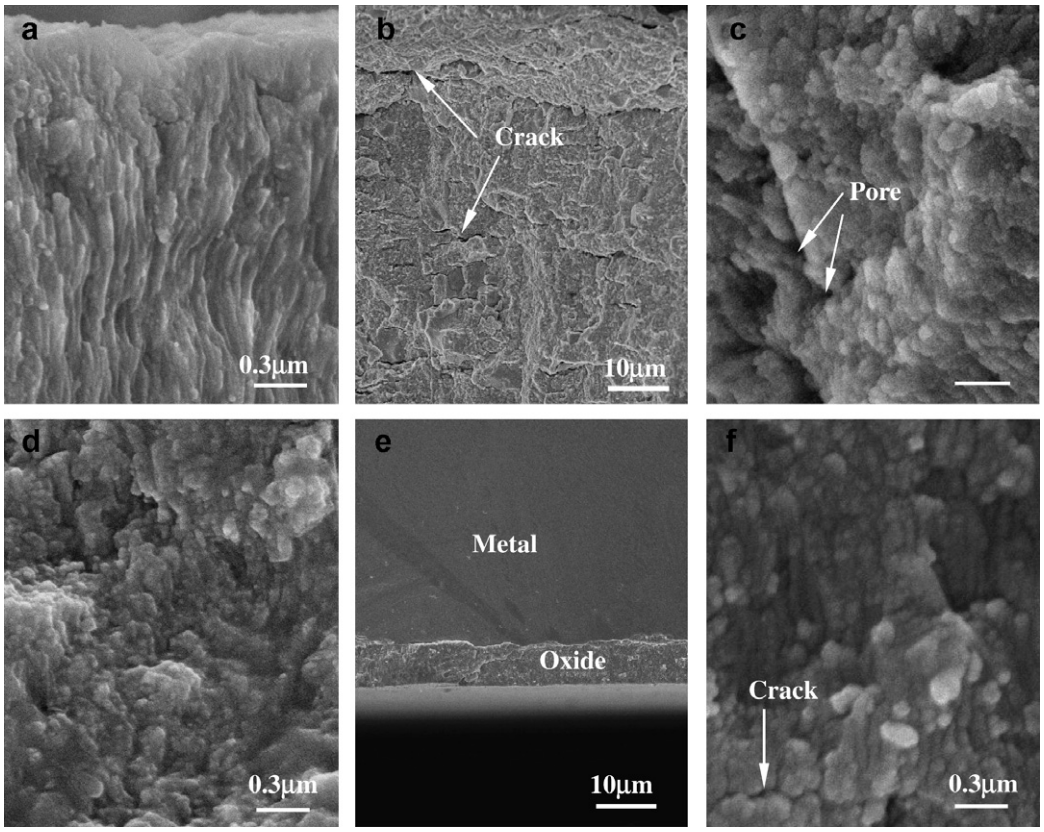

Fig. 4. The fracture surface morphology of the oxide films formed in 360 °C lithiated water observed by HRSEM. The upper interface in the figures refers to the metal/oxide interface: (a–c) RA Zry-4 specimen for 100 days (a) and 210 days (b and c) at different magnifications; (d–f) βQ Zry-4 specimen for 100 days (d) and 210 days (e and f) at different magnifications.

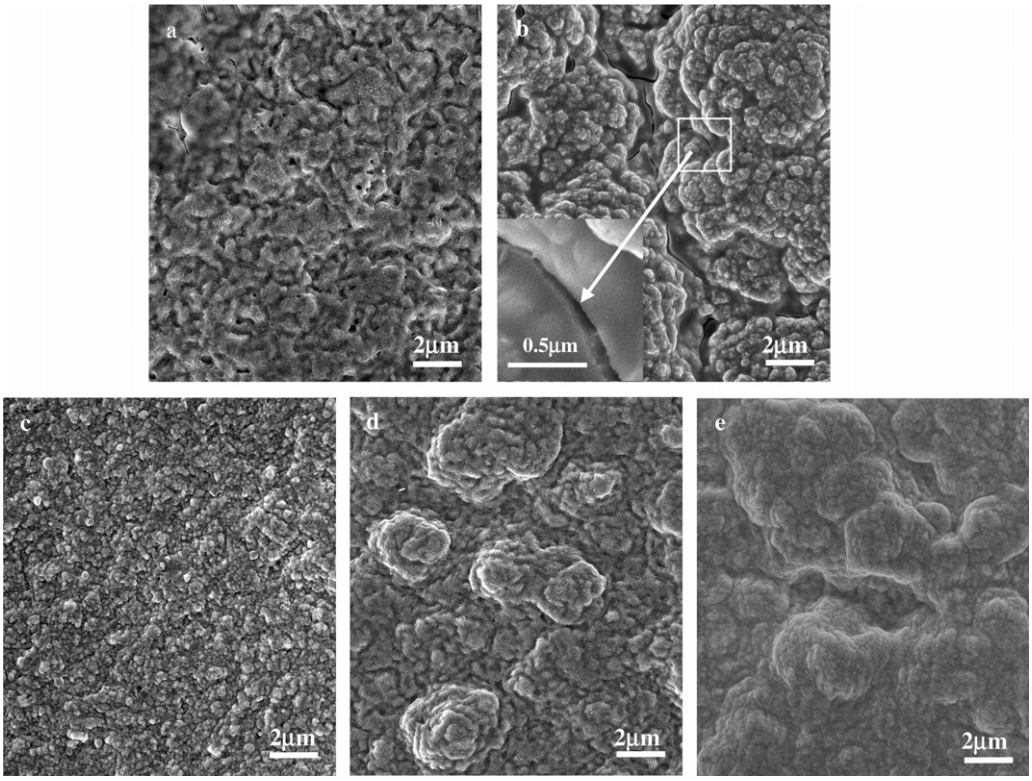

Fig. 5. The inner surface morphology of the oxide films formed in 360 °C lithiated water observed by HRSEM: (a and b) RA Zry-4 specimen for 100 days and 210 days, respectively and (c–e) βQ Zry-4 specimen for 100 days, 210 days and 300 days, respectively.

of observed cracks must present either as cracks or weak boundaries in the oxide film before sample preparation. Obviously, solution-treatment of the βQ Zry-4 specimen noticeably slows down the development of pores to cracks in the oxide film.

Moreover, the transformation from columnar grains to equiaxed grains is evident for RA Zry-4 specimen (Fig. 4(a) and (c)). However, it is not evident for βQ Zry-4 specimen and equiaxed grains are observed dominantly regardless of corroding time (Figs. 4(d) and (f)). The equiaxed grains are less than 100 nm in both specimens for 210 days exposure.

3.3.2. Inner surface morphology of oxide films

Fig. 5 shows the inner surface morphology of oxide films on RA Zry-4 and βQ Zry-4 specimens corroded for different time, respectively. Here, the micro-pores observed in oxide films are believed to be artifacts arising from the attack of the solution at SPPs during sample preparation due to their comparative size and slower oxidation of SPPs than the matrix. At the early stage of oxide growth (100 days exposure), a relatively planar inner surface is evident for both specimens with different heat-treatments (Fig. 5(a) and (c)). However, a typical 'cauliflower-like' morphology is evident at the later stage of oxide growth (Fig. 5(b), (d) and (e)), as observed in the post-transition oxide film on Zircaloy-2 tested in 400 °C steam [27] and on Zry-4 and ZIRLO tested in lithiated water and pure water, suggesting a typical inner surface morphology of the post-transition oxide film [21,26]. Obviously, the growth of oxide film is faster and more uneven for RA Zry-4 specimen than that for βQ Zry-4 specimen.

In addition, smooth regions and cracks on the inner surface of oxide films are more easily found in the RA Zry-4 specimen corroded for 210 days (Fig. 5(b)) than that in βQ Zry-4 specimen even corroded for 300 days (Fig. 5(e)). Note that the cracks in Fig. 5(b) are also likely artifacts resulting from the stress-relief after etching the metal matrix out during the sample preparation, but there exists a higher inner stress in the oxide film on RA Zry-4 specimen than βQ Zry-4 specimen. The smooth regions are likely an amorphous phase (see the bottom left corner in Fig. 5(b), which is a magnification of the rectangle area), which was also observed and indicated by Zhou in the examination of oxide films near the zirconium alloy matrix using TEM, SPM and HRSEM [21,26,28].

4. Discussion

4.1. The reason for improving corrosion resistance by the solution-treatment of β-quenching

Sabol et al. [8] investigated the effect of the β-quenching treatment before tube reduced extrusion (where also denoted as βQ Zry-4) on corrosion behavior of Zry-4 tube in lithiated water, and found the corrosion resistance of βQ Zry-4 tube was inferior to that of conventional Zry-4 one. It should be pointed out that the βQ Zry-4 tube in Ref. [8] actually underwent further intermediate recrystallization and a final stress-relief anneal after β-quenching ($\sum A_i = 1.1 \times 10^{-18}$ h). Zhou et al. [17] also investigated the corrosion behavior of βQ Zry-4 tube (in fact, the tubes were then cold-pilgered and stress-relief annealed at 470 °C for 4 h after β-quenching, $\sum A_i = 1.6 \times 10^{-23}$ h) in deionized water at 360 °C/18.6 MPa, and found that it possessed superior corrosion resistance in deionized water before 300 days exposure, but there was a second transition phenomenon at 300 days and the weight gain increased quickly after second transition. It was proposed that too low $\sum A_i$ value ($<2 \times 10^{-18}$ h) or fine SPPs (<0.05 μm) was not good for uniform corrosion resistance (autoclave testing in 350 °C water or PWRs [14], and it was reported that the corrosion resistance of Zry-4 in 350 °C water would go worse when the cooling rate exceeded 500 °C/s from β-Zr region [29]. In this study, however, βQ Zry-4 specimen with fine SPPs exhibits superior corrosion resistance and the accelerated second transition phenomenon does not appear even during a long-term exposure for 529 days, the weight gain of which is consistently comparable to that of ZIRLO and N18, while RA Zry-4 specimen with recommended $\sum A_i$ or SPPs size exhibits inferior corrosion resistance (Fig. 3). This illustrates that the SPPs size should not be the reason for improving the corrosion resistance by the solution-treatment of β-quenching.

As mentioned in Section 1, the heat-treatments also vary the contents of alloying elements in α-Zr matrix besides the SPPs size. The results from EDS analysis show that there is no difference in Sn content, but there is obvious difference in Fe and Cr contents in α-Zr matrix of βQ Zry-4 and RA Zry-4 specimens; The contents of Fe + Cr in α-Zr matrix reach 1400 μg/g in βQ Zry-4 specimen, which are much higher than those in RA Zry-4 specimen (see Table 1). The results are close to Li's [19], who analyzed the Fe and Cr contents in α-Zr matrix with a combination method of extracting electrochemically $Zr(Fe,Cr)_2$ particles from Zry-4 and analyzing mass concentration in electrolyte by means of flame atomic absorption spectrometry. Wadman and Andrén [18] also analyzed the matrix composition of Zry-4 with different heat-treatments using atom probe analysis and studied their corrosion behavior in 400 °C steam. Results also showed that Zry-4 with higher iron concentration in the matrix exhibited the best uniform corrosion resistance. In addition, it was found that β-quenching treatment employed at later period in fabricating Zircaloy tubes was a benefit for improving the nodular corrosion resistance [17,30], which was attributed to an increase in the amount of alloying elements retained in α-Zr matrix. Meanwhile, based on a fact that Nb has a higher solid solubility in α-Zr matrix, Zr–Sn–Nb (e.g. ZIRLO and N18) alloys exhibit superior corrosion resistance in lithiated water (Fig. 2). Thus, it can be concluded that the increase of Fe and Cr contents in α-Zr matrix resulting from β-quenching treatment is responsible for the excellent corrosion resistance of βQ Zry-4 specimen in lithiated water.

4.2. The relationship between the corrosion behavior and the microstructure of oxide films

Corrosion behavior is closely associated with the oxide characteristics, such as oxide grain shapes, pores and cracks in the oxide. Generally, the increase in the fraction of the columnar grains is corresponding to the lower weight gain and corrosion rate and the transformation from columnar grains to equiaxed grains is suggested to associate with the corrosion transition [12,31–33]. This seems true for RA Zry-4 specimen (Fig. 4(a)–(c)), however, the columnar grains are almost not evident in the oxide layer on βQ Zry-4 specimen with superior corrosion resistance (Fig. 4(d)–(f)). Wadman et al. [34] reported columnar grains were still observed besides equiaxed grains even in a thick oxide layer. This shows that the shapes of the oxide grains may not be correlated consequentially to the corrosion behavior.

The cracks in the oxide film on βQ Zry-4 specimen is much less than those on RA Zry-4 specimen, the development of pores to cracks on the former is noticeably slower than that on the latter (Fig. 4), and the growth of oxide film is slower and less uneven for the former than that for the latter (Fig. 5), which is corresponding to their corrosion behavior. In investigating the effect of alloying composition on the microstructure evolution of oxide films on zirconium alloys tested in lithiated water, Zhou et al. [26] also found that the pore clusters and micro-cracks along grain boundaries were more easily formed in the oxide film on Zry-4 than ZIRLO, and the cracks parallel to the oxide/metal interface were also more easily produced in the former than that in the latter. This illustrates that the increase in solute contents of alloying elements in α-Zr matrix, whether it is obtained by adding alloying elements with higher solid solubility (e.g. adding Nb in Zry-4) or by heat-treatments (e.g. β-quenching of Zry-4 in this study), is beneficial for retarding the development of pores to cracks, thereby improve the corrosion resistance. The possible reason is that the alloying elements in α-Zr matrix are easier than those in SPPs to dissolve in ZrO_2 during oxidation. It is known that Sn has much higher solid solubility in α-Zr matrix than Fe, Cr and Nb do, however, higher Sn content is detrimental for the corrosion resistance. Therefore, the effect of alloying elements in α-Zr matrix on the growth of oxide films needs to be further investigated.

5. Conclusion

(1) β-quenching treatment increases the contents of Fe and Cr in α-Zr matrix of Zry-4 alloy to about 700 μg/g, respectively, which are much higher than their maximal solubility in α-Zr matrix.
(2) After treated by β-quenching, Zry-4 specimens show excellent corrosion resistance in lithiated water, the weight gain of which is consistently comparable to that of ZIRLO and N18 alloys during 529 days exposure. The increase of Fe and Cr contents in α-Zr matrix is responsible for the improvement of corrosion resistance by β-quenching.
(3) The fracture surface and inner surface morphology of oxide films shows that β-quenching treatment significantly slows down the development of pores to cracks in oxide films and reduces the uneven growing tendency of the oxide, which is related to the corrosion behavior.

Acknowledgements

This project is financially supported by the National Nature Science Foundation of China (50371052) and Shanghai Leading Academic Discipline Project (T0101).

References

[1] B. Cox, Y.M. Wong, in: Zirconium in the Nuclear Industry: Ninth International Symposium, ASTM STP, vol. 1132, 1991, p. 643.
[2] D. Pêcheur, J. Godlewski, et al., in: Zirconium in the Nuclear Industry: Twelfth International Symposium, ASTM STP, vol. 1354, 2000, p. 793.
[3] B.X. Zhou, Q. Li, Q. Huang, et al., Nucl. Power Eng. 21 (5) (2000) 439 (in Chinese).
[4] N. Ramasubramanian, N. Precoanin, V.C. Ling, in: Zirconium in the Nuclear Industry: Eighth International symposium, ASTM STP, vol. 1023, 1989, p. 187.
[5] I.L. Bramwell, P.D. Parsons, D.R. Tice, in: Zirconium in the Nuclear Industry: Ninth International Symposium, ASTM STP, vol. 1132, 1991, p. 628.
[6] P. Billot, S. Yagnik, N. Ramasubramanian, et al., in: Zirconium in the Nuclear Industry: Thirteenth International Symposium, ASTM STP, vol. 1423, 2002, p. 169.
[7] G.P. Sabol, G.R. Kilp, et al., in: Zirconium in the Nuclear Industry: Eighth International Symposium, ASTM STP, vol. 1023, 1989, p. 227.
[8] G.P. Sabol, R.J. Comstock, et al., in: Zirconium in the Nuclear Industry: Tenth International Symposium, ASTM STP, vol. 1245, 1994, p. 724.
[9] W.J. Zhao, Z. Miao, et al., J. Chin. Soc. Corros. Protect. 22 (2) (2002) 124 (in Chinese).
[10] A.V. Nikulina, V.A. Markelvo, et al., in: Zirconium in the Nuclear Industry: Eleventh International Symposium, ASTM STP, vol. 1295, 1996, p. 785.
[11] Y.H. Jeong, K.O. Lee, H.G. Kim, J. Nucl. Mater. 302 (2002) 9.
[12] H. Anada, B.J. Herb, et al., in: Zirconium in the Nuclear Industry: Eleventh International Symposium, ASTM STP, vol. 1295, 1996, p. 74.
[13] P. Foster, J. Dougherty, M.G. Burke, et al., J. Nucl. Mater. 173 (2) (1990) 164.
[14] F. Garzarolli, E. Steinberg, H.G. Weidinger, in: Zirconium in the Nuclear Industry: Eighth International Symposium, ASTM STP, vol. 1023, 1989, p. 202.
[15] D. Charquet, R. Hahn, et al., in: Zirconium in the Nuclear Industry: Eighth International Symposium, ASTM STP, vol. 1023, 1989, p. 405.
[16] T. Thorvaldsson, T. Andersson, et al., in: Zirconium in the Nuclear Industry: Eighth International Symposium, ASTM STP, vol. 1023, 1989, p. 128.
[17] B.X. Zhou, W.J. Zhao, Z. Miao, et al., China Nuclear Science and Technology Report, CNIC-01074, SINRE-0066, 1996.
[18] B. Wadman, H.Q. Andrén, in: Zirconium in the Nuclear Industry: Eighth International Symposium, ASTM STP, vol. 1023, 1989, p. 423.
[19] C. Li, B.X. Zhou, W.J. Zhao, et al., J. Nucl. Mater. 304 (2002) 134.

[20] C.M. Eucken, P.T. Finden, et al., in: Zirconium in the Nuclear Industry: Eighth International Symposium, ASTM STP, vol. 1023, 1989, p. 113.
[21] B.X. Zhou, Q. Li, M.Y. Yao, et al., Nucl. Power Eng. 26 (4) (2005) 364 (in Chinese).
[22] B. Cox, M. Ungurela, et al., in: Zirconium in the Nuclear Industry: Eleventh International Symposium, ASTM STP, vol. 1295, 1996, p. 114.
[23] H.J. Beie, A. Mitwalsky, F. Garazorlli, et al., in: Tenth International Symposium, ASTM STP, vol. 1245, 1994, p. 615.
[24] N. Ramasubramanian, in: Zirconium in the Nuclear Industry: Ninth International Symposium, ASTM STP, vol. 1132, 1991, p. 613.
[25] N. Ramasubramanian, P.V. Balakrishnan, in: Zirconium in the Nuclear Industry: Tenth International Symposium, ASTM STP, vol. 1245, 1994, p. 378.
[26] B.X. Zhou, Q. Li, W.Q. Liu, et al., Rare Met. Mater. Eng. 35 (7) (2006) 1009 (in Chinese).
[27] G. Wikmark, P. Ruding, et al., in: Zirconium in the Nuclear Industry: Eleventh International Symposium, ASTM STP, vol. 1295, 1996, p. 55.
[28] B.X. Zhou, Q. Li, M.Y. Yao, et al., Rare Met. Mater. Eng. 32 (6) (2003) 417 (in Chinese).
[29] F. Garzarolli, I. Pohlmeyer, et al., External cladding corrosion in water power reactors, in: Proceeding of a Technical Committee Meeting, International Atomic Energy Agency, Cadarache, France, 1985, p. 66.
[30] T. Kubo, M. Uno, in: Zirconium in the Nuclear Industry: Ninth International Symposium, ASTM STP, vol. 1132, 1991, p. 476.
[31] D. Pêcheur, J. Godlewski, et al., in: Zirconium in the Nuclear Industry: Eleventh International Symposium, ASTM STP, vol. 1295, 1996, p. 94.
[32] H. Anada, K. Takeda, in: Zirconium in the Nuclear Industry: Tenth International Symposium, ASTM STP, vol. 1295, 1996, p. 35.
[33] A. Yilmazbayhan, E. Breval, et al., J. Nucl. Mater. 349 (2006) 265.
[34] B. Wadman, Z. Lei, et al., in: Zirconium in the Nuclear Industry: Tenth International Symposium, ASTM STP, vol. 1245, 1994, p. 579.